EurJIC European Journal of Inorganic Chemistry

FULL PAPER

DOI: 10.1002/ejic.201200197

Bis(pyrazol-1-yl)methane as Non-Chromophoric Ancillary Ligand for Charged Bis-Cyclometalated Iridium(III) Complexes

Sheng Meng,*[a] Il Jung,[b] Jie Feng,[a] Rosario Scopelliti,[b] Davide Di Censo,[b] Michael Grätzel,[b] M. Khaja Nazeeruddin,[b] and Etienne Baranoff*[b,c]

Keywords: Iridium / Luminescence / Density functional calculations / Pyrazole / Molecular modeling

New charged cyclometalated iridium(III) complexes $[Ir(ppy)_2(L)](PF_6)$ [ppy = 2-phenylpyridine; L = bis(pyrazol-1-yl)methane (for **1**); L = bis(3,5-dimethylpyrazol-1-yl)methane (for **2**)] were synthesized and their electrochemical and photophysical properties studied. These complexes with non-π-electron-conjugated ancillary chelates exhibit significantly blue-shifted emission relative to those of commonly used derivatives with N^N ancillary ligands such as bipyridine or phenanthroline. Both X-ray and theoretical analysis based on time-dependent density functional theory (TD-DFT) reveal that the binding of Ir to the bis(pyrazol-1-yl)methane ancillary ligand is much weaker than that to the phenylpyridine main ligand; the effect is enhanced in the excited state. As a result, the ancillary ligand does not participate in low-energy excitations and triplet emission, and the electronic transitions are concentrated on the main chromophoric ligands. The blueshift feature is attributed to emission originating from the main cyclometalated ligands, in contrast to emitters with the N^N chromophoric ancillary ligand. In addition, complex **2** exhibits a one order of magnitude higher non-radiative decay rate than complex **1**, which is attributed to the steric hindrance of the methyl groups that leads to a more loosely bound ancillary ligand.

Introduction

Because of their unique photophysical properties,[1–3] cyclometalated iridium complexes have attracted widespread interest in recent years.[4–18] While mostly neutral complexes have been studied, mainly for organic light-emitting diodes (OLEDs), charged complexes are particularly appealing for light-emitting electrochemical cells (LECs).[19–23] There are major advantages of LECs over OLEDs originating from the use of mobile ions. Under applied voltage, the ions migrate towards the electrodes causing a local drop in potential, which facilitates charge injections in the device. Multilayer architectures necessary for charge injection and transport in OLEDs are therefore not necessary in LECs, which makes their industrial production promisingly easier.

The most commonly used design for charged iridium emitters is based on heteroleptic bis-cyclometalated iridium complexes with a neutral N^N ancillary ligand, which leads to positively charged complexes. Various N^N ligands have been used such as bipyridines,[24,25] phenanthrolines,[26,27] pyridine-pyrazole,[28] pyridine-imidazole,[22] pyridine-triazole,[23] pyridine-tetrazole.[29] In all those complexes, however, the lowest unoccupied molecular orbital (LUMO) is largely localized on the N^N ancillary ligand as a result of the direct link between the two N-heterocyclic rings, which results in a lower LUMO relative to those of the cyclometalated phenyl-pyridine ligands. The ancillary ligand therefore forms a five-membered metallacycle with the central iridium ion. Unfortunately, this approach limits the preparation of charged deep blue emitters. Only a pyridine-carbene ancillary ligand has the necessary high-lying LUMO for deep blue emission from charged iridium(III) complexes that have an ancillary ligand that forms a five-membered metallacycle.[30]

Herein we report the utilization of bis(pyrazol-1-yl)methane as a neutral N^N ancillary ligand. In this case, the ancillary ligand forms a six-membered metallacycle with the central iridium ion, a similar geometry to that of the previously reported bispyridyl-amine,[31] and biscarbene complexes.[32] Because of the presence of the non-conjugated methylene bridge, no delocalization occurs over the two rings, which greatly increases the triplet energy of the ancillary ligand.[33] As a consequence, the LUMO of the complexes is now localized on the main ligand and the emission properties are mainly governed by the C^N ligand. With this approach, the complex $[Ir(ppy)_2\{(pz)_2CH_2\}]^+$ [ppy = 2-phenylpyridine and $(pz)_2CH_2$ = bis(pyrazol-1-yl)methane] emits at 476 nm, significantly blueshifted from the emission of $[Ir(ppy)_2(bpy)]^+$ at 585 nm (bpy = 2,2′-bipyridine)[34] and similar to those of previously reported complexes $[Ir(ppy)_2$-

[a] Beijing National Laboratory for Condensed Matter Physics, and Institute of Physics, Chinese Academy of Sciences, 100190 Beijing, China
E-mail: smeng@iphy.ac.cn
[b] Laboratory of Photonics and Interfaces, École Polytechnique Fédérale de Lausanne, 1015 Lausanne, Switzerland
[c] School of Chemistry, University of Birmingham, Edgbaston, B15 2TT, England
E-mail: e.baranoff@bham.ac.uk

(pypz)]$^+$ at 475 nm [pypz = 2-(pyrazol-1-yl)pyridine],[28] [Ir(ppy)$_2$(pybim)]$^+$ at 471 nm [pybim = 3-methyl-1-(4-methylpyridin-2-yl)-1*H*-benzo[*d*]imidazol-3-ium],[30] and [Ir(tpy)$_2$-{(pz)$_3$CH}]$^+$ at 476 nm [tpy = 2-tolylpyridine and (pz)$_3$CH = tri(pyrazol-1-yl)methane] (Scheme 1).[35] Our results are rationalized using extensive density functional theory (DFT) and time-dependent DFT (TDDFT) calculations; we find that Ir binding to bis(pyrazol-1-yl)methane is much weaker than to the main phenylpyridine ligands, especially in the excited state. Orbital analysis shows that the bis(pyrazol-1-yl)methane ligand is not involved in low-energy excitation and does not directly contribute to the emission processes, thus is nonchromophoric. Its presence ensures that the electrons are further localized onto the main phenylpyridine ligands, which results in a significant blueshift of the triplet emission relative to those of previous complexes employing aromatic ancillary ligands. Interestingly, when there are methyl substituents on the bispyrazole ancillary ligand, the nonradiative decay rate increases by one order of magnitude, which results in a very poor photoluminescence quantum yield. This is attributed to the more loosely bound ancillary ligand than for the complex without methyl groups.

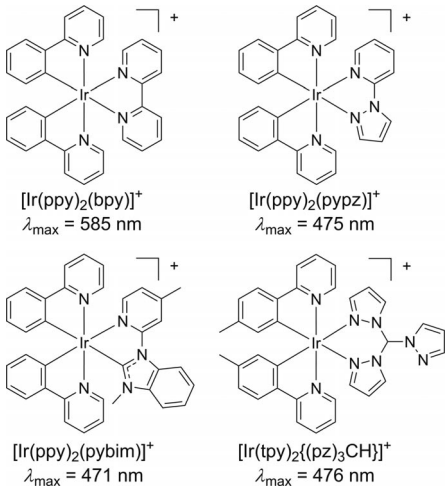

Scheme 1. Previously reported complexes.

Results and Discussion

The two ancillary ligands of complexes **1** and **2** (Scheme 2) have been synthesized as previously reported in the literature by reacting dichloromethane with the required pyrazole derivative in the presence of tetrabutylammonium hydrogen sulfate, potassium hydroxide, and potassium carbonate.[36] The chlorido-bridged iridium dimer [Ir(ppy)$_2$(μ-Cl)]$_2$ was swiftly synthesized within 3 h by using the iridium(I) dimer [Ir(COD)(μ-Cl)]$_2$ as starting material.[37] Further reaction with the ancillary ligands in dichloromethane heated at reflux followed by anion exchange with KPF_6 led to complexes **1** and **2** in fair yield (68% and 54%, respectively). The complexes were characterized by ^{1}H NMR spectroscopy, high-resolution mass spectrometry, and elemental analysis (see Experimental Section for details). Interestingly, the ^{1}H NMR spectra show that the complexes are symmetric in solution with 11 and 9 aromatic signals for **1** and **2**, respectively, and a singlet for the methylene-bridge. This points to a flexible methylene bridge on the NMR timescale.

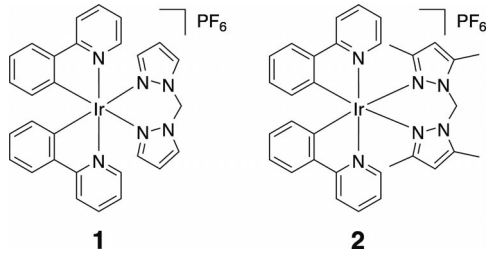

Scheme 2. Chemical structures of complexes **1** and **2**.

Single crystals of **1** suitable for X-ray diffraction analysis were grown by slow diffusion of hexane in a dichloromethane solution of the complex. The structure is shown in Figure 1, and selected bond lengths and angles are reported in Table 1. The complex exhibits an expected slightly distorted octahedral geometry around the iridium center with the two pyridine-rings in *trans* position to each other. The flexible methylene-bridge forces the two pyrazole groups to be non-coplanar. Furthermore, the N–Ir–N bite angle of the ancillary ligand, 87.90(6)°, is significantly larger than those for previously reported complexes with ancillary ligands that form a five-membered metallacycle with the central iridium atom, approximately 76°.

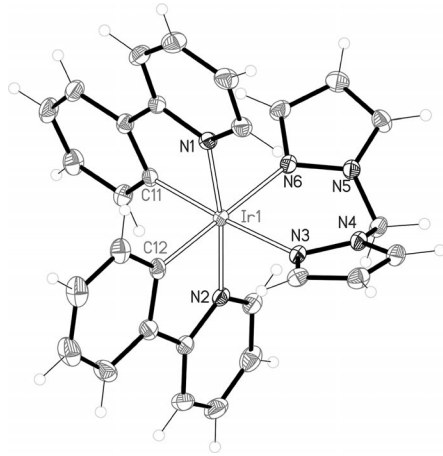

Figure 1. ORTEP drawing of complex **1**.

The UV/Vis absorption spectra of **1** and **2** recorded in acetonitrile solution are reported in Figure 2. They display intense absorption bands ($\varepsilon \approx 3.8 \times 10^4$ M^{-1} cm^{-1}) in the UV region. These bands are assigned to ligand-centered (LC) ^{1}-(π–π*) transitions from the cyclometalated ligand 2-phenylpyridine. The weaker ($\varepsilon \approx 4000$ M^{-1} cm^{-1}) bands at lower energies (350–440 nm) are assigned to metal-to-ligand charge-transfer (MLCT) transitions.[38] Finally, weak absorption bands ($\varepsilon \approx 220$ M^{-1} cm^{-1}) are observed at 466 and 468 nm for **1** and **2**, respectively. They correspond to direct singlet–triplet transitions.[39] When the acetonitrile solution of the

Table 1. Selected bond lengths [Å] and angles [°] for **1** and calculated structural parameters for **1** and **2**.

		1		**2**	
	X-ray	S_0	T_1	S_0	T_1
Distances					
Ir1–N1	2.0516(17)	2.09	2.10	2.08	2.09
Ir1–N2	2.0464(17)	2.08	2.05	2.08	2.06
Ir1–C11	2.0051(19)	2.02	2.01	2.02	2.01
Ir1–C12	2.011(2)	2.02	1.99	2.02	1.99
Ir1–N3	2.1679(16)	2.26	2.31	2.35	2.38
Ir1–N6	2.1552(17)	2.26	2.28	2.33	2.34
Angles					
N1–Ir1–C11	80.44(7)	80.11	80.16	80.23	80.20
N1–Ir1–N2	172.04(6)	173.28	174.87	172.24	174.55
N3–Ir1–N6	87.90(6)	85.44	84.37	84.89	84.34
N6–Ir1–C11	91.48(7)	93.56	93.85	97.05	97.00

complexes are excited at a wavelength that falls within the π–π* and MLCT absorption regions, the complexes **1** and **2** show structured emission with maxima at 477 and 486 nm, respectively, and a clear vibronic progression of about 1200 cm^{-1} (Figure 2). At 77 K, the emission spectra show intense and highly resolved bands with very small rigidochromism compared to the emission at room temperature. In addition to the small Stokes shift (less than 20 nm), these results point to a weak MLCT character of the triplet excited state, which is therefore largely of ligand-centered (^{3}LC) character.

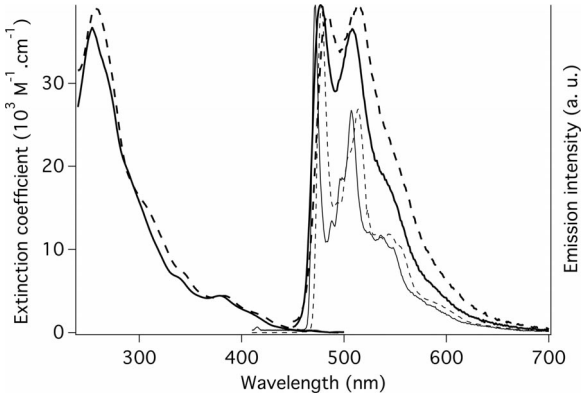

Figure 2. Absorption (left) and emission (right) spectra of **1** (full lines) and **2** (dashed lines) in acetonitrile solution at room temperature (thick lines) and 77 K (thin lines).

The photoluminescence quantum yields (Φ) and lifetimes of the excited state (τ) of the complexes in solution in acetonitrile at room temperature are reported in Table 2. Complex **1** exhibits a quantum yield of 0.21 and τ of 0.67 μs, whereas complex **2** has a low quantum yield of only 1.4% and τ of 34 ns. Nevertheless, the radiative constants are similar for the two complexes, 3.1×10^5 and 4.1×10^5 s^{-1}. On the other hand, the nonradiative constant is one order of magnitude higher for **2** than for **1**. This is attributed to the methyl substituents on the ancillary ligand, which induces a stronger distortion in the ground and excited state geometry of **2** relative to **1**. This, in turn, opens new nonradiative deactivation pathways. This effect is similar to the reported impact of the 6,6′-substitution of bipyridine by phenyl groups, which enhances the deactivation pathways through accessible metal-centered ^{3}MC states.[40]

Table 2. Photophysical and electrochemical properties of **1** and **2**.

	λ_{abs}[a] [nm]	λ_{em}[b] [nm]	λ_{em}[c] [nm]	Φ	τ [ns]	k_r 10^{-5} [s^{-1}][d]	k_{nr} 10^{-5} [s^{-1}][d]	E_{ox}[e] [V]
1	254, 378	477	472	0.21	669	3.14	11.8	0.92
2	258, 382	484	478	0.014	34	4.12	290	0.92

[a] Acetonitrile solution at room temperature. [b] Oxygen-free acetonitrile solution at room temperature. [c] 2-methyltetrahydrofuran at 77 K. [d] By assuming unitary intersystem crossing, $k_r = \Phi/\tau$ and $k_{nr} = (1 - \Phi)/\tau$. [e] In acetonitrile, vs. Fc^+/Fc, with a glassy carbon electrode and tetrabutylammonium hexafluorophosphate (0.1 M) as supporting electrolyte.

Finally the oxidation potentials were measured in acetonitrile with 0.1 M $TBAPF_6$ as supporting electrolyte and are reported vs. the ferrocenium/ferrocene couple in Table 2. They are attributed to the oxidation of the metal center as is usually observed for this class of compounds. They are the same for the two complexes, 0.92 V vs. Fc^+/Fc, which shows the negligible impact of the substitution of the ancillary ligand on the oxidation potential of the complex.

To provide insight into the electronic structure, photoabsorption and emission properties of the two complexes, we performed first-principles calculations within density functional theory and time-dependent DFT.[41,42] We employed the SIESTA code[43] to investigate the ground-state geometry of complex **1** and **2** by optimizing bond lengths until the force on each atom is smaller than 0.04 eV/Å in magnitude. During geometry optimization, we used Troullier–Martins pseudopotentials[44] to represent the atomic cores, the generalized gradient approximation for the exchange-correlation functional,[45] and a double-ξ plus polarization basis of localized orbitals with an energy cut-off of 120 Ry. We also used the Gaussian09 program package[46] and the B3YLP exchange-correlation functional to calculate the energy levels of the molecular orbitals for both complexes, as well as the photoabsorption and emission spectra. The 6-31G(d) basis sets were used for light elements, and the LANL2DZ basis for iridium metal. This set of parameters has been tested to produce good agreement with the measured photospectroscopic data for organic dyes.[47]

The optimized geometry parameters of complex **1** in the ground state and the first excited state are listed in Table 1. The values of the important bond lengths and bond angles, in general, agree well with the values measured from X-ray crystallography. For instance, the calculated angles centered at the Ir^{III} ion X–Ir–Y (X = C, N; Y = C, N) are within 3° of those obtained experimentally; in particular, the chelation angle of the ancillary ligand, N(3)–Ir–N(6), is 85.44° as compared to 87.90° measured by X-ray diffraction, which is much larger than the chelation angle of the aromatic ancillary ligand in previously reported complexes. In comparison with the X-ray data, the bond lengths in the first-principles calculations are systematically overestimated by 0.04–0.10 Å, presumably because of the choice of the Ir pseudopotential. Fortunately, the trends in the bond lengths determined experimentally and by theoretical calculations agree

very well with each other. The Ir–C bond is shorter than the Ir–N bond in the phenylpyridine component, while the N atoms in the bis(pyrazol-1-yl)methane ancillary ligand forms much longer bonds (by 0.1–0.15 Å) with the Ir^{III} ion. It is worth noting that on going to complex **2**, the distances Ir–N3 and Ir–N6 increase significantly by about 0.08 Å (Table 1). It shows that the introduction of bulky methyl groups result in a loosely bound ancillary ligand.

The geometry in the first excited state, calculated from TDDFT, does not show significant changes in bond lengths and bond angles. The bond lengths change by about 0.01–0.05 Å, and the angles change by less than 2°. This is consistent with the trends in other complexes. However, the N3–Ir–N6 angle in the bis(pyrazol-1-yl)methane ligand is now 1.08° smaller upon excitation, and the Ir–C/Ir–N bond lengths in phenylpyridine is also shortened by ~0.03 Å. On the other hand, the Ir–N bonds for the bis(pyrazol-1-yl)-methane ligand are elongated by 0.01–0.05 Å. Both indicate that the excited state involves stronger Ir–phenylpyridine bonding and weaker Ir–ligand bonding. This would lead to a blue emission that is concentrated on the phenylpyridine components of the complex, as a result of the charge repulsion by the nonaromatic bis(pyrazol-1-yl)methane ligand.

The electronic structure and corresponding wavefunctions for molecular orbitals in complex **1** and **2** are displayed in Figures 3 and 4. The highest occupied molecular orbital (HOMO) for complex **1** is located at –7.86 eV relative to the vacuum level, and it is separated from the HOMO–1 states by 0.60 eV. The energy level for the LUMO of complex **1** is –4.07 eV, and the LUMO+1 state is 0.08 eV higher in energy. The energy gap between the HOMO and the LUMO is 3.79 eV (327.2 nm). Our calculation of the optical absorption spectrum indicates that the small bump at 380 nm and the main absorption peak have significant contributions from electronic transitions between these states. Electrons in the HOMO and HOMO–1 are distributed on the two phenylpyridine C^N ligands symmetrically, while electrons in the LUMO and LUMO+1 are mainly localized on one of the C^N ligands with a π orbital character. It is interesting that the distribution of the LUMO and LUMO+1 states on the C^N ligand are almost identical, but on different phenylpyridine groups. The loose character of the binding between Ir^{III} and the bis(pyrazol-1-yl)methane ligand prohibits any significant distribution of electron density onto the bis(pyrazol-1-yl)methane ligand for the molecular orbitals of the HOMO, HOMO-1 and LUMO, LUMO+1 states, as shown in Figure 3. This results in a blueshifted absorption and photoemission relative to those in other complexes without the bis(pyrazol-1-yl)methane ligands as previously studied.

The electronic structure and molecular orbital distribution for complex **2**, displayed in Figure 4, is very similar to those of complex **1**. The HOMO state is located at –7.78 eV, and the HOMO–1 state is 0.56 eV below. The energy gap between the HOMO and LUMO states is 3.77 eV (328.9 nm). All these numbers are close to those of complex **1** (difference within 0.05 eV). The redshift of the HOMO–LUMO energy gap from complex **1** to **2** is about 0.02 eV

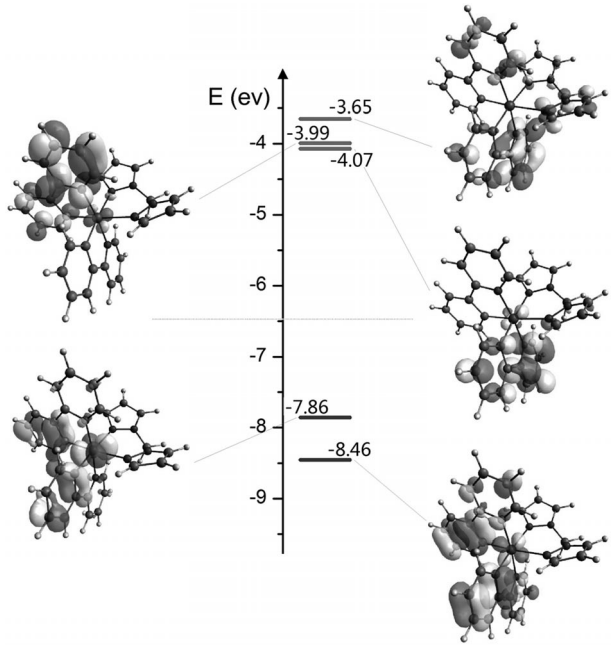

Figure 3. Electronic energy levels and corresponding molecular orbitals for complex **1**.

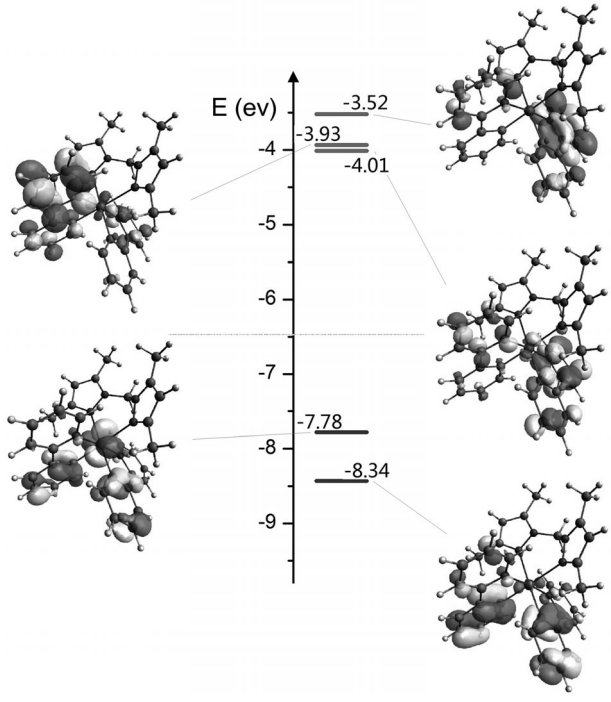

Figure 4. Electronic energy levels and corresponding molecular orbitals for complex **2**.

(and ~2 nm), while experimentally the main absorption peaks are redshifted by 4 nm, because of the presence of the two methane groups on the edge of the bis(pyrazol-1-yl)methane ancillary ligand. Similarly, the HOMO and HOMO–1 of complex **2** are also localized on the C^N phenylpyridine ligands symmetrically, and the LUMO and LUMO+1 have electrons localized at one of the two C^N

ligands with π orbital character. In addition, the LUMO and LUMO+1 states are very close in energy, lying within 0.08 eV of each other.

For a straightforward justification and comparison to experiment, Figure 5 shows the calculated absorption and emission spectra for complex **1** and **2** from TDDFT. In the photoabsorption spectra, there appear three major absorption peaks for complex **1**, with the peak maximum located at around 402, 306, and 265 nm. The corresponding values for complex **2** are 408, 314, and 267 nm, respectively, all redshifted from those for complex **1**, which results from electron delocalization due to the presence of additional methane groups in the periphery of the bis(pyrazol-1-yl)-methane ligand for complex **2**. By comparing with the values obtained experimentally, the peak at ~400 nm corresponds to the measured small bump at ~380 nm for both complexes; the difference between them is assigned to the inaccuracy of the exchange-correlation functional and pseudopotentials used in the computational models. The main peak at 265 nm (267 nm) also nicely agrees with the measured value at 254 nm (258 nm) for complex **1** (complex **2**). The shoulder at around 310 nm is less pronounced in the spectrum obtained experimentally, but it is still discernible (Figure 2). In their first excited state (spin triplet), both complexes **1** and **2** emit at a wavelength of ~448 nm. The emission spectra for complexes **1** and **2** are almost identical, as shown in Figure 5. This value can be compared to the experimentally measured emission peak at 470–480 nm. Vibronic couplings, exhibited in the measured spectra in Figure 2, are not taken into consideration in the theoretical modeling, and thus they do not show up in Figure 5.

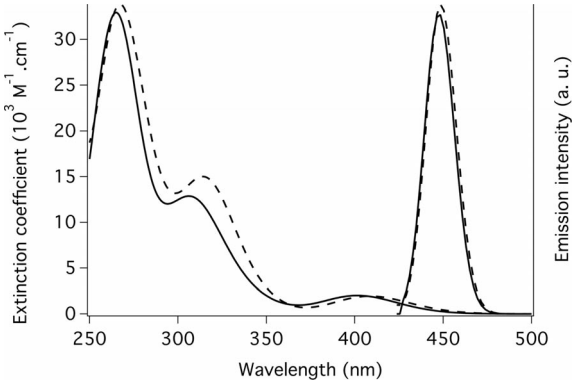

Figure 5. Calculated absorption (left) and emission (right) spectra of complex **1** (full line) and **2** (dashed line).

To provide some information on the electronic distribution of the excited states, we show, in Figure 6, a direct comparison of the molecular orbitals in the ground-state geometry and the first excited-state geometry for both complexes **1** and **2**. The distribution of the molecular orbitals is very close to each other in the ground state and the excited state. The only significant difference, shown in Figure 6(d), is that the LUMO is distributed on both C^N phenylpyridine ligands in the ground state of complex **2**, while in the excited state, the LUMO is further localized on only one of the C^N phenylpyridine ligand. This implies that the electrons in the excited states of the complexes are more localized, which results in a stronger MLCT character and lower MLCT excitation energy with a long emission wavelength. Furthermore, it is important to emphasize that none of the HOMO and LUMO levels involve participation from the ancillary ligand, neither in the ground state nor in the excited state.

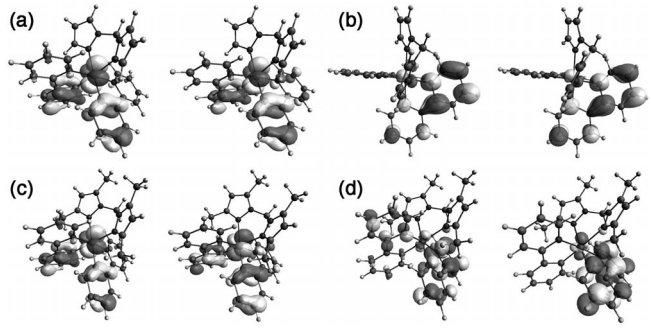

Figure 6. Comparison of the molecular orbitals between the ground state and excited state of both complexes **1** and **2**. (a) The HOMO of complex **1**, ground state (left) and excited state (right). (b) The LUMO of complex **1**, ground state (left) and excited state (right). (c) The HOMO of complex **2**, ground state (left) and excited state (right). (d) The LUMO of complex **2**, ground state (left) and excited state (right).

Conclusions

We report new nonchromophoric ancillary ligands for charged bis-cyclometalated iridium(III) complexes. The methylene bridge in bis(pyrazol-1-yl)methane prevents delocalization over the two rings and results in weaker metal–ligand binding in the excited state, which significantly increases the triplet energy of the ancillary ligand. As a consequence, the emission properties of the complexes are mainly governed by the C^N ligand, in contrast to those for commonly designed charged complexes based on chromophoric N^N ancillary ligands. With this strategy, complex **1** $[Ir(ppy)_2((pz)_2CH_2)]^+$ [ppy = 2-phenylpyridine and $(pz)_2CH_2$ = bis(pyrazol-1-yl)methane] emits at 476 nm, which is significantly blueshifted relative to that of $[Ir(ppy)_2(bpy)]^+$ at 585 nm (bpy = 2,2′-bipyridine). This work calls attention to the potential of the bis(pyrazol-1-yl)methane ancillary ligands for shifting the emission of charged complexes towards the blue. Furthermore, it hints at the impact of the ancillary ligand on the nonradiative decay rate constant, which could help design new phosphorescent iridium(III) complexes with photophysically improved properties.

Experimental Section

General: Solvents were of puriss grade and used as received. The ligands bis(pyrazol-1-yl)methane and bis(3,5-dimethyl-pyrazol-1-yl)methane were prepared as reported in the literature.[34] $[Ir(ppy)_2(\mu\text{-}Cl)]_2$ was prepared from $[Ir(COD)(\mu\text{-}Cl)]_2$ as previously reported.[35] ^1H spectra were recorded by using a Bruker AV 400 MHz spectrometer. Chemical shifts δ (in ppm) are referenced

to residual solvent peaks. Coupling constants are expressed in Hertz [Hz].

Complex 1: Bis(pyrazol-1-yl)methane (72 mg, 0.486 mmol) was added to a solution of $[Ir(ppy)_2(\mu\text{-}Cl)]_2$ (200 mg, 0.186 mmol) in dichloromethane (50 mL), and the mixture was stirred under reflux for 8 h. Addition of solid KPF_6 (204 mg, 1.1 mmol) and methanol (10 mL) followed by the removal of dichloromethane under vacuum resulted in a yellow precipitate, which was filtered through fritted glass, washed with methanol and deionized water, and dried under vacuum. The solid was dissolved in a small amount of dichloromethane (about 3 mL) and poured into ethyl ether. The precipitate was filtered off, washed with ethyl ether, and dried. Complex **1** was obtained as a pale yellow solid (201 mg, 68% yield). ^{1}H NMR (CD_3CN): δ = 8.07 (dd, J = 8.0, 0.9 Hz, 2 H), 8.02 (dd, J = 2.7, 0.7 Hz, 2 H), 7.93 (s br., 2 H), 7.90 (ddd, J = 8.9, 7.4, 1.5 Hz, 2 H), 7.75 (dd, J = 7.9, 1.1 Hz, 2 H), 7.15 (ddd, J = 7.4, 5.9, 1.4 Hz, 2 H), 7.01 (ddd, J = 8.9, 7.7, 1.2 Hz, 2 H), 6.97 (dd, J = 2.2, 1.6 Hz, 2 H), 6.88 (td, J = 7.4, 1.4 Hz, 2 H), 6.41 (s, 2 H), 6.37 (t, J = 2.48 Hz, 2 H), 6.27 (dt, J = 7.6, 0.6 Hz, 2 H) ppm. ESI-HRMS: *m*/*z* calcd. for $C_{29}H_{24}IrN_6$ $[M - PF_6]^+$ 649.1693; found 649.1649. $C_{29}H_{24}F_6IrN_6P$ (793.73): calcd. C 43.88, H 3.05, N 10.59; found C 43.57, H 3.12, N 10.45.

Complex 2: The procedure was similar to that of complex **1**, but by using bis(3,5-dimethyl-pyrazol-1-yl)methane (100 mg, 0.487 mmol). Complex **2** was obtained as a pale yellow solid (171 mg, 54% yield). ^{1}H NMR ($CDCl_3$): δ = 8.19 (s br., 2 H), 7.89 (dd, J = 8.1, 1.0 Hz, 2 H), 7.85 (dt, J = 7.2, 1.4 Hz, 2 H), 7.55 (dd, J = 7.8, 1.0 Hz, 2 H), 7.23 (t, J = 6.2 Hz, 2 H), 6.90 (dt, J = 7.6, 1.1 Hz, 2 H), 6.72 (dt, J = 7.6, 1.4 Hz, 2 H), 6.23 (dd, J = 7.7, 0.8 Hz, 2 H), 6.18 (s, 2 H), 5.84 (s, 2 H), 6.90 (dt, J = 7.6, 1.1 Hz, 2 H), 2.49 (s, 6 H), 1.22 (s, 6 H) ppm. ESI-HRMS: *m*/*z* calcd. for $C_{33}H_{32}IrN_6$ $[M - PF_6]^+$ 705.2319; found 705.2304. $C_{33}H_{32}F_6IrN_6P{\cdot}0.25C_4H_{10}O$: calcd. C 47.03, H 4.00, N 9.68; found C 46.75, H 4.02, N 9.58.

Photophysical Properties: UV/Vis spectra were recorded in a 1-cm pathlength quartz cell on a Cary 100 spectrophotometer. Emission spectra were recorded on a Fluorolog 3–22 by using a 90° optical geometry. The quantum yields were determined by using fluorescein (10^{-5} M in 0.1 M NaOH; air equilibrated; QY = 0.93) as standard.[48] Excited-state lifetimes were measured by using a FL-1061PC TCSPC instrument and 406 nm Nanoled as excitation source. Solutions were degassed by bubbling argon gently for 30 min.

Electrochemistry: A PC-controlled AutoLab PSTAT10 electrochemical workstation was employed. Cyclic voltammograms were obtained at a scan rate of 100 mV/s by using 0.1 M $TBAPF_6$ as supporting electrolyte in acetonitrile. Glassy carbon, sputtered platinum, and platinum wire were employed as working, counter, and reference electrodes, respectively. At the end of each measurement, the ferrocenium/ferrocene (Fc^+/Fc) potential was measured and used as an internal reference.

X-ray Crystal Structure Determination: The data for compound **1** was measured at low temperature [140(2) K] by using Mo-K_α radiation on an Oxford Diffraction KM4/Sapphire CCD quipped with a kappa geometry goniometer. The data was reduced by CrysAlisPro[49] and then corrected for absorption.[50] Solution and refinement were performed by SHELX.[51] The structure was refined by using full-matrix least-squares based on F^2 with all non-hydrogen atoms anisotropically defined. Hydrogen atoms were placed in calculated positions by means of the "riding" model. $C_{29}H_{24}F_6IrN_6P$, M_w = 793.71, orthorhombic, space group *Pbca*, a = 10.77207(17), b = 16.9574(3), c = 30.5558(4) Å, V = 5581.51(15) Å^3, Z = 8, $d_{calcd.}$ = 1.889 g cm^{-3}, F (000) = 3088, 54548 reflections collected (6888 independent), R_{int} = 0.0228, GOF on F^2 = 1.044, R_1 = 0.0172 [$I > 2\sigma(I)$], wR_2 = 0.0397 (all data). CCDC-869000 contains the supplementary crystallographic data for this paper. These data can be obtained free of charge from The Cambridge Crystallographic Data Centre via www.ccdc.cam.ac.uk/data_request/cif.

Acknowledgments

This work was supported by the Hundred-Talent Program of CAS, the National Natural Science Foundation of China (NSFC) (grant 11074287), MOST (2012CB921403), and the European Union (CELLO, STRP 248043).

[1] L. Flamigni, A. Barbieri, C. Sabatini, B. Ventura, F. Barigelletti, *Top. Curr. Chem.* **2007**, *281*, 143–203.
[2] E. Baranoff, J. H. Yum, M. Graetzel, M. K. Nazeeruddin, *J. Organomet. Chem.* **2009**, *694*, 2661–2670.
[3] Y. You, S. Y. Park, *Dalton Trans.* **2009**, 1267–1282.
[4] C. Ulbricht, B. Beyer, C. Friebe, A. Winter, U. S. Schubert, *Adv. Mater.* **2009**, *21*, 4418–4441.
[5] M. S. Lowry, S. Bernhard, *Chem. Eur. J.* **2006**, *12*, 7970–7977.
[6] W.-Y. Wong, C.-L. Ho, *Coord. Chem. Rev.* **2009**, *253*, 1709–1758.
[7] S. K. Leung, K. Y. Kwok, K. Y. Zhang, K. K. W. Lo, *Inorg. Chem.* **2010**, *49*, 4984–4995.
[8] Q. Zhao, S. J. Liu, F. Y. Li, T. Yi, C. H. Huang, *Dalton Trans.* **2008**, 3836–3840.
[9] M. Schmittel, H. W. Lin, *Inorg. Chem.* **2007**, *46*, 9139–9145.
[10] M. Marin-Suarez del Toro, J. F. Fernandez-Sanchez, E. Baranoff, M. K. Nazeeruddin, M. Graetzel, A. Fernandez-Gutierrez, *Talanta* **2010**, *82*, 620–626.
[11] K. K. W. Lo, J. S. Y. Lau, *Inorg. Chem.* **2007**, *46*, 700–709.
[12] H. Sato, K. Tamura, M. Taniguchi, A. Yamagishie, *New J. Chem.* **2010**, *34*, 617–622.
[13] Y. S. Yeh, Y. M. Cheng, P. T. Chou, G. H. Lee, C. H. Yang, Y. Chi, C. F. Shu, C. H. Wang, *ChemPhysChem* **2006**, *7*, 2294–2297.
[14] W. Y. Lai, J. W. Levell, A. C. Jackson, S. C. Lo, P. V. Bernhardt, I. D. W. Samuel, P. L. Burn, *Macromolecules* **2010**, *43*, 6986–6994.
[15] B. Lou, Z. Q. Chen, Z. Q. Bian, C. H. Huang, *New J. Chem.* **2010**, *34*, 132–136.
[16] J.-H. Jou, M.-F. Hsu, W.-B. Wang, C.-L. Chin, Y.-C. Chung, C.-T. Chen, J.-J. Shyue, S.-M. Shen, M.-H. Wu, W.-C. Chang, C.-P. Liu, S.-Z. Chen, H.-Y. Chen, *Chem. Mater.* **2009**, *21*, 2565–2567.
[17] D. Li, F. F. Chen, Z. Q. Bian, Z. W. Liu, Y. L. Zhao, C. H. Huang, *Polyhedron* **2009**, *28*, 897–902.
[18] K. Saito, Y. Sarukawa, K. Tsuge, T. Konno, *Eur. J. Inorg. Chem.* **2010**, 3909–3913.
[19] J. D. Slinker, A. A. Gorodetsky, M. S. Lowry, J. J. Wang, S. Parker, R. Rohl, S. Bernhard, G. G. Malliaras, *J. Am. Chem. Soc.* **2004**, *126*, 2763–2767.
[20] S. Graber, K. Doyle, M. Neuburger, C. E. Housecroft, E. C. Constable, R. D. Costa, E. Orti, D. Repetto, H. J. Bolink, *J. Am. Chem. Soc.* **2008**, *130*, 14944–14945.
[21] J. L. Rodriguez-Redondo, R. D. Costa, E. Orti, A. Sastre-Santos, H. J. Bolink, F. Fernandez-Lazaro, *Dalton Trans.* **2009**, 9787–9793.
[22] L. He, J. Qiao, L. Duan, G. F. Dong, D. Q. Zhang, L. D. Wang, Y. Qiu, *Adv. Funct. Mater.* **2009**, *19*, 2950–2960.
[23] M. Mydlak, C. Bizzarri, D. Hartmann, W. Sarfert, G. Schmid, L. De Cola, *Adv. Funct. Mater.* **2010**, *20*, 1812–1820.
[24] W.-Y. Wong, G.-J. Zhou, X.-M. Yu, H.-S. Kwok, Z. Lin, *Adv. Funct. Mater.* **2007**, *17*, 315–323.
[25] Q. Zhao, M. X. Yu, L. X. Shi, S. J. Liu, C. Y. Li, M. Shi, Z. G. Zhou, C. H. Huang, F. Y. Li, *Organometallics* **2010**, *29*, 1085–1091.

[26] C. Rothe, C. J. Chiang, V. Jankus, K. Abdullah, X. S. Zeng, R. Jitchati, A. S. Batsanov, M. R. Bryce, A. P. Monkman, *Adv. Funct. Mater.* **2009**, *19*, 2038–2044.
[27] X. S. Zeng, M. Tavasli, I. F. Perepichka, A. S. Batsanov, M. R. Bryce, C. J. Chiang, C. Rothe, A. P. Monkman, *Chem. Eur. J.* **2008**, *14*, 933–943.
[28] L. He, L. Duan, J. Qiao, R. J. Wang, P. Wei, L. D. Wang, Y. Qiu, *Adv. Funct. Mater.* **2008**, *18*, 2123–2131.
[29] S. Stagni, S. Colella, A. Palazzi, G. Valenti, S. Zacchini, F. Paolucci, M. Marcaccio, R. Q. Albuquerque, L. De Cola, *Inorg. Chem.* **2008**, *47*, 10509–10521.
[30] F. Kessler, R. D. Costa, D. Di Censo, R. Scopelliti, E. Ortí, H. J. Bolink, S. Meier, W. Sarfert, M. Grätzel, M. K. Nazeeruddin, E. Baranoff, *Dalton Trans.* **2012**, *41*, 180–191.
[31] M. C. Tseng, W. L. Su, Y. C. Yu, S. P. Wang, W. L. Huang, *Inorg. Chim. Acta* **2006**, *359*, 4144–4148.
[32] C. H. Yang, J. Beltran, V. Lemaur, J. Cornil, D. Hartmann, W. Sarfert, R. Frohlich, C. Bizzarri, L. De Cola, *Inorg. Chem.* **2010**, *49*, 9891–9901.
[33] Y.-H. Song, Y.-C. Chiu, Y. Chi, Y.-M. Cheng, C.-H. Lai, P.-T. Chou, K.-T. Wong, M.-H. Tsai, C.-C. Wu, *Chem. Eur. J.* **2008**, *14*, 5423–5434.
[34] R. D. Costa, E. Orti, H. J. Bolink, S. Graber, S. Schaffner, M. Neuburger, C. E. Housecroft, E. C. Constable, *Adv. Funct. Mater.* **2009**, *19*, 3456–3463.
[35] J. Li, P. I. Djurovich, B. D. Alleyne, M. Yousufuddin, N. N. Ho, J. C. Thomas, J. C. Peters, R. Bau, M. E. Thompson, *Inorg. Chem.* **2005**, *44*, 1713–1727.
[36] L. D. Field, B. A. Messerle, M. Rehr, L. P. Soler, T. W. Hambley, *Organometallics* **2003**, *22*, 2387–2395.
[37] E. Baranoff, B. F. E. Curchod, J. Frey, R. Scopelliti, F. Kessler, I. Tavernelli, U. Rothlisberger, M. Grätzel, M. K. Nazeeruddin, *Inorg. Chem.* **2012**, *51*, 215–224.
[38] B. Schmid, F. O. Garces, R. J. Watts, *Inorg. Chem.* **1994**, *33*, 9–14.
[39] E. Baranoff, B. F. E. Curchod, F. Monti, F. Steimer, G. Accorsi, I. Tavernelli, U. Rothlisberger, R. Scopelliti, M. Grätzel, M. K. Nazeeruddin, *Inorg. Chem.* **2012**, *51*, 799–811.
[40] R. D. Costa, F. Monti, G. Accorsi, A. Barbieri, H. J. Bolink, E. Orti, N. Armaroli, *Inorg. Chem.* **2011**, *50*, 7229–7238.
[41] W. Kohn, L. J. Sham, *Phys. Rev.* **1965**, *140*, A1133–A1138.
[42] E. Runge, E. K. U. Gross, *Phys. Rev. Lett.* **1984**, *52*, 997–1000.
[43] J. M. Soler, E. Artacho, J. D. Gale, A. Garcia, J. Junquera, P. Ordejon, D. Sanchez-Portal, *J. Phys. Condens. Matter* **2002**, *14*, 2745–2779.
[44] N. Troullier, J. L. Martins, *Phys. Rev. B* **1991**, *43*, 1993–2006.
[45] J. P. Perdew, K. Burke, M. Ernzerhof, *Phys. Rev. Lett.* **1996**, *77*, 3865–3868.
[46] M. J. Frisch, *Gaussian 09*, Gaussian, Inc., Wallingford CT, **2009**.
[47] S. Meng, E. Kaxiras, M. K. Nazeeruddin, M. Grätzel, *J. Phys. Chem. C* **2011**, *115*, 9276–9282.
[48] J. Shen, R. D. Snook, *Chem. Phys. Lett.* **1989**, *155*, 583–586.
[49] *CrysalisPro*, Oxford Diffraction Ltd., **2010**.
[50] R. H. Blessing, *Acta Crystallogr., Sect. A* **1995**, *51*, 33–38.
[51] G. M. Sheldrick, *Acta Crystallogr., Sect. A* **2008**, *64*, 112–122.

Received: February 27, 2012
Published Online: May 18, 2012

